Exact Robot Navigation Using Power Diagrams

Omur Arslan and Daniel E. Koditschek

***Abstract*— We reconsider the problem of reactive navigation in sphere worlds, i.e., the construction of a vector field over a compact, convex Euclidean subset punctured by Euclidean disks, whose flow brings a Euclidean disk robot from all but a zero measure set of initial conditions to a designated point destination, with the guarantee of no collisions along the way. We use power diagrams, generalized Voronoi diagrams with additive weights, to identify the robot's collision free convex neighborhood, and to generate the value of our proposed candidate solution vector field at any free configuration via evaluation of an associated convex optimization problem. We prove that this scheme generates a continuous flow with the specified properties. We also propose its practical extension to the nonholonomically constrained kinematics of the standard differential drive vehicle.**

I. Introduction

Among the many proposed methods of motion planning in cluttered environments [1], [2], one actively researched approach to reactive planners tackles the robot navigation problem by attempting simultaneously to solve the motion planning and control problems via the evaluation of a closed loop vector field. In this paper, we introduce a new construction for such feedback planners using tools from computational geometry and convex optimization that have been more traditionally associated with roadmap-style approaches. In so doing, our construction raises the possibility of a "doubly reactive," scheme mixing some of the advantages of sensor-based exploration [3] with those of hybrid real-time control [4] in that not merely the integrated robot trajectory, but also its generating vector field can be constructed on the fly in real time.

A. Motivation and Prior Literature

The simple, computationally efficient artificial potential field[1] approach to real-time obstacle avoidance [5] incurs topologically necessary critical points [6], which, in practice, with no further remediation often include (topologically unnecessary) spurious local minima. Actually constructively removing these spurious attractors, e.g., via *navigation functions* [7], or other methods [8] [2] has largely come at the price of complete prior information and has been restricted to topologically simple settings.

Extensions to the navigation function framework partially overcoming the necessity of global prior knowledge of (and consequent parameter tuning for) a topologically and metrically simple environment [9], [10], and controlling nonholonomically constrained kinematic systems [11], [12] have appeared in the last decade. Sequential composition [13] has been used to cover metrically complicated environments with convex cell-based local potential decompositions [4] (and extended to nonholonomically constrained finite size robots [14]), but still necessitating prior global knowledge of the environment.

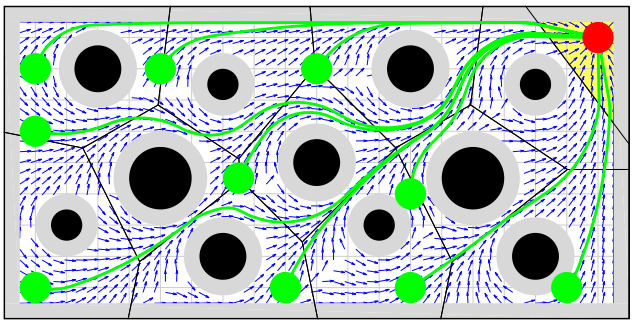

Fig. 1. Exact robot navigation using power diagrams, generated by disks representing obstacles (black) and the robot (red at the goal). The power cell (yellow) associated with the robot defines its obstacle free convex local neighborhood, and the continuous feedback motion towards the metric projection of a given desired goal (red) onto this convex set asymptotically steers almost all robot configurations (green) to the goal without collisions along the way. The grey regions represent the augmented workspace boundary and obstacles, and the arrows show the direction of the resulting vector field.

B. Contributions and Organization of the Paper

This paper abandons the smooth potential field approach to reactive planning, constructing a piecewise smooth vector field with the same capabilities as navigation functions for topologically and metrically simple environments (i.e., "sphere worlds" [15]), but relaxing the assumption of global prior knowledge. We use power diagrams — generalized Voronoi diagrams with additive weights [16] — to identify a collision free convex neighborhood of a robot configuration, and solve the safe navigation problem via continuous evaluation of an associated convex optimization problem. Our construction requires no parameter tuning and requires only local knowledge of the environment in the sense that the sensor needs only locate proximal obstacles — those whose power cells are adjacent[3] to the robot's. The proposed

The authors are with the Department of Electrical and Systems Engineering, University of Pennsylvania, Philadelphia, PA 19104. E-mail: {omur, kod}@seas.upenn.edu. This work was supported by AFOSR under the CHASE MURI FA9550-10-1-0567.

[1] We adopt standard usage to denote by this term the use of the negative gradient field of a scalar valued function as the force or velocity control law for a fully actuated, kinematic (first order dynamics) robot.

[2] It bears mentioning that harmonic functions are utilized to design potential functions without local minima [8]; however, such intrinsically numerical constructions forfeit the reactive nature of feedback motion planners under discussion here.

[3] A pair of power cells in $\mathbb{R}^N$ are said to be adjacent if they share a $N-1$ dimensional face.

vector field generates a smooth flow with a unique attractor at the specified goal location along with (the topologically necessary number of) saddles — one associated with each obstacle. Since all of its critical points are nondegenerate, our vector field is guaranteed to steer almost all collision free robot configurations to the goal location while avoiding collisions along the way, as illustrated in Fig. 1. We extend the practicability of the result by adapting the fully actuated point particle vector field planner to the widely used kinematic differential drive vehicle model (retaining the convergence and collision avoidance guarantees, at the necessary cost of a discontinuous feedback law). [4] [5]

This paper is organized as follows. Section II continues with a formal statement of the problem at hand. In Section III we briefly summarize some important properties of power diagrams and introduce their use for identifying collision free robot configurations. Section IV, comprising the central contribution of the paper, constructs the navigation vector field for a metric sphere world [15]. Section V demonstrates the effectiveness of the proposed navigation algorithm using numerical simulations. We conclude in Section VI with a summary of our contributions and a brief discussion of future work.

II. Problem Formulation

For ease of exposition [6] we restrict our attention to a disk-shaped robot, centered at $\mathrm{x} \in \mathcal{W}$ with radius $r \in \mathbb{R}_{\geq 0}$, operating in a closed compact convex environment $\mathcal{W}$ in $\mathbb{R}^N$ punctured with $n \in \mathbb{N}$ open disks, centered at $\mathbf{p} := (\mathrm{p}_1, \mathrm{p}_2, \ldots, \mathrm{p}_n) \in \mathcal{W}^n$ with a vector of radii $\boldsymbol{\rho} := (\rho_1, \rho_2, \ldots, \rho_n) \in (\mathbb{R}_{>0})^n$, representing obstacles.[7] Hence, the free space $\mathcal{F}$ of the robot is defined as

$$\mathcal{F} := \left\{ \mathrm{x} \in \mathcal{W} \,\middle|\, \overline{B(\mathrm{x}, r)} \subseteq \mathcal{W} \setminus \bigcup_{i=1}^{n} B(\mathrm{p}_i, \rho_i) \right\}, \quad (1)$$

where $B(\mathrm{p}, \rho) := \left\{ \mathrm{q} \in \mathbb{R}^N \,\middle|\, \|\mathrm{q} - \mathrm{p}\| < \rho \right\}$ is the open ball of radius $\rho \in \mathbb{R}_{\geq 0}$ centered at $\mathrm{p} \in \mathbb{R}^N$, and $\overline{B(\mathrm{p}, \rho)}$ denotes its closure, and $\|.\|$ denotes the standard Euclidean norm.

To guarantee the connectivity of the free space $\mathcal{F}$, we assume that our disk-shaped robot can go around any obstacle in any direction throughout the workspace $\mathcal{W}$: [8]

Assumption 1 *Obstacles are separated from each other by clearance of at least*

$$\|\mathrm{p}_i - \mathrm{p}_j\| > \rho_i + \rho_j + 2r \quad \forall i \neq j, \quad (2)$$

and from the boundary $\partial\mathcal{W}$ of the workspace $\mathcal{W}$ as

$$\min_{\mathrm{q} \in \partial\mathcal{W}} \|\mathrm{q} - \mathrm{p}_i\| > \rho_i + 2r, \quad \forall i. \quad (3)$$

Before formally stating our navigation problem, it is useful to recall the well known topological limitation of a continuous motion planner on a generalized sphere world: if a continuous vector field planner on a generalized sphere world has a unique attractor, then it must have at least as many saddles as obstacles [15]. In consequence, the robot navigation problem that we seek to solve is stated as:

Problem 1 *Assuming the first order (completely actuated single integrator) robot dynamics,*

$$\dot{\mathrm{x}} = \mathrm{u}(\mathrm{x}), \quad (4)$$

find a Lipschitz continuous vector field controller, $\mathrm{u} : \mathcal{F} \to \mathbb{R}^N$, that leaves the robot's free space $\mathcal{F}$ positively invariant, and asymptotically steers almost all robot configurations in $\mathcal{F}$ to any given goal location $\mathrm{x}^* \in \mathcal{F}$.

III. Encoding collisions via Power Diagrams

In this section, we list some important properties of power diagrams, and then describe how we use power diagrams to determine a safe neighborhood of a robot.

A. Power Diagrams

The power diagram $\mathcal{P}(\mathbf{p}, \boldsymbol{\rho}) = \{P_1, \ldots, P_n\}$ of a convex environment $\mathcal{W}$ in $\mathbb{R}^N$, based on a set of generator disks centered at $\mathbf{p} = (\mathrm{p}_1, \ldots, \mathrm{p}_n) \in \mathcal{W}^n$ with a vector of (*power*) radii $\boldsymbol{\rho} = (\rho_1, \ldots, \rho_n) \in (\mathbb{R}_{\geq 0})^n$, is a partition [9] of $\mathcal{W}$ such that every point $\mathrm{q} \in \mathcal{W}$ is assigned to the closest generator based on the *power distance*, $\|\mathrm{q} - \mathrm{p}_i\|^2 - \rho_i^2$, as [16]

$$P_i := \left\{ \mathrm{q} \in \mathcal{W} \,\middle|\, \|\mathrm{q} - \mathrm{p}_i\|^2 - \rho_i^2 \leq \|\mathrm{q} - \mathrm{p}_j\|^2 - \rho_j^2, \ \forall j \neq i \right\}. \quad (5)$$

A power diagram defines a convex cell decomposition of a convex environment, and the boundary ∂P_i of P_i is defined by the boundary $\partial\mathcal{W}$ of the workspace $\mathcal{W}$ and the separating hyperplane H_{ij} between power cells P_i and P_j for some $j \neq i$ [16]. The separating hyperplane H_{ij} between any pair $i \neq j$ of power cells P_i and P_j is perpendicular to the line joining p_i and p_j and passes through the point $\mathrm{h}_{ij} := \alpha_{ij}\mathrm{p}_i + (1 - \alpha_{ij})\mathrm{p}_j$, [10]

$$H_{ij} := \left\{ \mathrm{q} \in \mathbb{R}^N \,\middle|\, (\mathrm{q} - \mathrm{h}_{ij})^{\mathrm{T}} (\mathrm{p}_i - \mathrm{p}_j) = 0 \right\}, \quad (6)$$

where

$$\alpha_{ij} := \frac{1}{2} - \frac{\rho_i^2 - \rho_j^2}{2\|\mathrm{p}_i - \mathrm{p}_j\|^2}, \quad (7)$$

and the perpendicular distance of p_i to H_{ij} is given by

[4] Generalized Voronoi diagrams and cell decomposition methods are traditionally encountered in the design of roadmap methods [2], [3], [17]. A major distinction between our construction and these roadmap algorithms is that the latter typically seek a global, one-dimensional graphical representation of a robot's environment (independent of any specific configuration), whereas our approach uses the local open interior cells of the robot-obstacle-workspace power diagram to determine a locally safe neighborhood of a given free configuration.

[5] It is useful to note that our use of power partitions are motivated by another application of Voronoi diagrams in robotics for coverage control of distributed mobile sensor networks [18]–[21]

[6] As would be true of any vector field planner on a topological model space, if exact global information is available our results generalize to any star world or forest of stars using an analytic diffeomorphism of a star world to a generalized sphere world [7], [22].

[7] Here, $\mathbb{N}$ is the set of all natural numbers; $\mathbb{R}$ and $\mathbb{R}_{>0}$ ($\mathbb{R}_{\geq 0}$) denote the set of real and positive (nonnegative) real numbers, respectively; and $\mathbb{R}^N$ is the N-dimensional Euclidean space.

[8] Assumption 1 is equivalent to the "isolated" obstacles assumption of [7].

[9] Here we slightly abuse the standard notation, and refer to a collection of subsets of a set A with disjoint interiors whose union is A as its "partition".

[10] Here $\mathbf{A}^{\mathrm{T}}$ denotes the transpose of matrix $\mathbf{A}$

$$d(\mathrm{p}_i, H_{ij}) := \min_{\mathrm{q}\in H_{ij}} \|\mathrm{q}-\mathrm{p}_i\| = (1-\alpha_{ij})\|\mathrm{p}_i-\mathrm{p}_j\|, \quad (8a)$$

$$= \rho_i + \frac{(\|\mathrm{p}_i-\mathrm{p}_j\|-\rho_i)^2-\rho_j^2}{2\|\mathrm{p}_i-\mathrm{p}_j\|}. \quad (8b)$$

Note that a power diagram may yield empty power cells associated with some generators and/or some generators may not be contained in their nonempty power cells; and a negative value of $d(\mathrm{p}_i, H_{ij})$ indicates that p_i is not contained in P_i, i.e., $\mathrm{p}_i \notin P_i$ iff $d(\mathrm{p}_i, H_{ij}) < 0$ for some $j \neq i$ [21]. Also observe that $d(\mathrm{p}_i, H_{ij}) \geq \rho_i$ iff $\|\mathrm{p}_i-\mathrm{p}_j\| \geq (\rho_i+\rho_j)$.

B. A Safe Neighborhood of a Robot

Throughout the rest of the paper, we consider a disk-shaped robot, centered at $\mathrm{x} \in \mathcal{W}$ with radius $r \in \mathbb{R}_{\geq 0}$, moving in a closed compact convex environment $\mathcal{W} \subset \mathbb{R}^N$ populated with disk-shaped obstacles, centered at $\mathbf{p} \in \mathcal{W}^n$ with a vector of radii $\boldsymbol{\rho} \in (\mathbb{R}_{>0})^n$, satisfying Assumption 1. Since the workspace and robot radius is fixed, we suppress all mentions of the associated terms wherever convenient, in order to simplify the notation.

Using the robot and obstacles as generator disks of a power diagram of $\mathcal{W}$, we define the *local workspace*, $\mathcal{LW}(\mathrm{x})$, of the robot, illustrated in Fig. 2, as,

$$\mathcal{LW}(\mathrm{x}) := \left\{ \mathrm{q}\in\mathcal{W} \middle| \|\mathrm{q}-\mathrm{x}\|^2 - r^2 \leq \|\mathrm{q}-\mathrm{p}_i\|^2 - \rho_i^2 \quad \forall i \right\}. \quad (9)$$

Proposition 1 *A robot placement $\mathrm{x} \in \mathcal{W} \setminus \bigcup_{i=1}^n \{\mathrm{p}_i\}$ is collision free in $\mathcal{F}$ (1) if and only if the robot body is contained in $\mathcal{LW}(\mathrm{x})$,*

$$\mathrm{x} \in \mathcal{F} \iff \overline{B(\mathrm{x}, r)} \subseteq \mathcal{LW}(x). \quad (10)$$

Proof. Let $\hat{\mathbf{p}} = (\hat{\mathrm{p}}_0, \hat{\mathrm{p}}_1, \ldots, \hat{\mathrm{p}}_n) \in \mathcal{W}^{n+1}$ be a disk configuration in $\mathcal{W}$ with a vector of (power) radii $\hat{\boldsymbol{\rho}} = (\hat{\rho}_0, \hat{\rho}_1, \ldots, \hat{\rho}_n) \in (\mathbb{R}_{\geq 0})^{n+1}$ such that $\hat{\mathrm{p}}_0 = \mathrm{x}$, $\hat{\rho}_0 = r$, and $\hat{\mathrm{p}}_i = \mathrm{p}_i$, $\hat{\rho}_i = \rho_i$ for all $i \in \{1, 2, \ldots, n\}$; and let $\mathcal{P}(\hat{\mathbf{p}}, \hat{\boldsymbol{\rho}}) = \{P_0, P_1, \ldots, P_n\}$ be the associated power diagram of $\mathcal{W}$. Note that $\mathcal{LW}(\mathrm{x}) = P_0$.

The boundary $\partial\mathcal{LW}(\mathrm{x})$ of $\mathcal{LW}(\mathrm{x})$ is defined by the boundary $\partial\mathcal{W}$ of the workspace $\mathcal{W}$ and the separating hyperplane H_{0i} between convex power cells $\mathcal{LW}(\mathrm{x})$ and P_i for some $i \neq 0$; and, in general, any pair $i \neq j$ of the convex cells P_i and P_j are separated by the hyperlane H_{ij} [16]. Hence, using (1), (8), (9), and convexity of $\mathcal{P}(\hat{\mathbf{p}}, \hat{\boldsymbol{\rho}})$, we obtain the result as

$$\overline{B(\mathrm{x}, r)} \subseteq \mathcal{LW}(\mathrm{x}) \iff \begin{cases} \mathrm{x} \in \mathcal{LW}(\mathrm{x}), \\ d(\mathrm{x}, \partial\mathcal{LW}(\mathrm{x})) \geq r, \end{cases} \quad (11)$$

$$\underbrace{\iff}_{\substack{\text{by (8) and convexity} \\ \text{of } \mathcal{P}(\hat{\mathbf{p}}, \hat{\boldsymbol{\rho}})}} \begin{cases} \mathrm{x} \in \mathcal{LW}(\mathrm{x}), \\ d(\mathrm{x}, \partial\mathcal{W}) \geq r, \\ d(\mathrm{x}, H_{0i}) \geq r \quad \forall i \neq 0, \end{cases} \quad (12)$$

$$\underbrace{\iff}_{\text{by (8) and (9)}} \begin{cases} \mathrm{x} \in \mathcal{W}, \\ d(\mathrm{x}, \partial\mathcal{W}) \geq r, \\ \|\mathrm{x}-\mathrm{p}_i\|^2 \geq (\rho_i^2 - r^2) \quad \forall i \neq 0, \\ \|\mathrm{x}-\mathrm{p}_i\| \geq (r+\rho_i) \quad \forall i \neq 0, \end{cases} \quad (13)$$

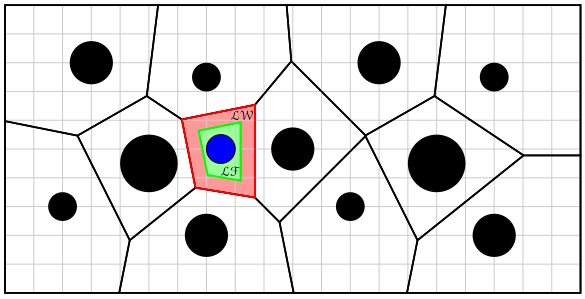

Fig. 2. Local workspace $\mathcal{LW}$ (red) and local free space $\mathcal{LF}$ (green) of a robot (blue). To construct its local free space and so its local workspace, the robot only requires to locate the four nearby obstacles whose power cells are adjacent[3] to the robot's power cell (i.e., local workspace).

$$\underbrace{\iff}_{\substack{\text{by convexity of } \mathcal{W} \\ (r+\rho_i) \geq \sqrt{|r^2-\rho_i^2|}}} \begin{cases} \overline{B(\mathrm{x}, r)} \subseteq \mathcal{W} \\ \|\mathrm{x}-\mathrm{p}_i\| \geq (r+\rho_i) \quad \forall i \neq 0, \end{cases} \quad (14)$$

$$\underbrace{\iff}_{\text{by (1)}} \mathrm{x} \in \mathcal{F}. \qquad \blacksquare$$

To determine a collision free neighborhood of the robot, we define the robot's *local free space*, $\mathcal{LF}(\mathrm{x})$, by eroding $\mathcal{LW}(\mathrm{x})$, removing the volume swept along its boundary, $\partial\mathcal{LW}(\mathrm{x})$, by the robot body radius, illustrated in Fig. 2, as [23] [11]

$$\mathcal{LF}(\mathrm{x}) := \mathcal{LW}(\mathrm{x}) \setminus \left(\partial\mathcal{LW}(\mathrm{x}) \oplus B(\mathbf{0}, r)\right), \quad (15a)$$

$$= \left\{ \mathrm{q} \in \mathcal{LW}(\mathrm{x}) \middle| \overline{B(\mathrm{q}, r)} \subseteq \mathcal{LW}(\mathrm{x}) \right\}. \quad (15b)$$

Note that $\mathcal{LF}(\mathrm{x})$ is a nonempty closed convex set, because $\mathrm{x} \in \mathcal{LF}(\mathrm{x})$ and the erosion of a closed convex set by an open ball is a closed convex set.[12]

Lemma 1 *Any robot configuration in the local free space $\mathcal{LF}(x)$ of a collision free robot location $\mathrm{x} \in \mathcal{F}$ is also collision free, i.e., $\mathcal{LF}(\mathrm{x}) \subseteq \mathcal{F}$ for all $\mathrm{x} \in \mathcal{F}$.*

Proof. The lemma directly follows from that $\mathcal{LW}(\mathrm{x})$ is an element of the power diagram of $\mathcal{W}$ generated by the robot and obstacles, as discussed in the proof of Proposition 1. $\blacksquare$

In the sequel, we shall design a vector field controller assuming knowledge of the robot's local free space and so its local workspace. To construct its local workspace, the robot only needs to locate its nearby obstacles whose power cells are adjacent[3] to the robot's local workspace. This can be achieved by assuming an adjustable radius sensory footprint and gradually increasing its sensing range until the set of obstacles in the sensing range satisfies a certain geometric criterion guaranteeing that the detected obstacles

[11] Here, $\mathbf{0}$ is a vector of all zeros with the appropriate size, and $A \oplus B$ denotes the Minkowski sum of sets A and B defined as $A \oplus B = \{a+b \mid a \in A, b \in B\}$.

[12] It is obvious that the erosion of a closed half-space by an open ball is a closed half-space. Hence, since the erosion operation is distributed over set intersection [23], and a closed convex set can be defined as (possibly infinite) intersection of closed half-spaces [24], and an arbitrary intersection of closed sets is closed [25], the erosion of a closed convex set by an open ball is a closed convex set.

exactly defines the robot's local workspace [18]. We leave a comprehensive detailed study of constructing the robot's local workspace to a future discussion of specific sensor model selections such as a fixed radius sensory footprint and/or a (limited range) line-of-sight sensor.

IV. Robot Navigation via Power Diagrams

In this section, we introduce a new provably correct vector field controller for safe robot navigation in a locally sensed metric sphere world (Problem 1), and list its important qualitative properties. We also present its extension for the nonholonomically constrained kinematic differential drive robot model.

A. Feedback Robot Motion Planner

For a choice of a desired goal location $\mathrm{x}^* \in \mathcal{F}$, we propose a robot navigation strategy that steers the robot $\mathrm{x} \in \mathcal{F}$ towards the global goal x^* through a safe local target location, called *"projected goal"*, that solves the following convex optimization problem,

$$\begin{aligned} &\text{minimize} \quad \|\mathrm{q}-\mathrm{x}^*\|^2 \\ &\text{subject to} \quad \mathrm{q} \in \mathcal{LF}(\mathrm{x}) \end{aligned} \tag{16}$$

where $\mathcal{LF}(\mathrm{x})$ (15) is the local free space around the robot location x and is a nonempty closed convex set. It is well known that the unique solution of (16) is given by [24, Section 8.1.1][13]

$$\overline{\mathrm{x}}^* := \begin{cases} \mathrm{x}^* & \text{, if } \mathrm{x}^* \in \mathcal{LF}(\mathrm{x}), \\ \Pi_{\mathcal{LF}(\mathrm{x})}(\mathrm{x}^*) & \text{, otherwise,} \end{cases} \tag{17}$$

where $\Pi_C(\mathrm{q})$ denotes the metric projection of $\mathrm{q} \in \mathbb{R}^N$ onto a convex set $C \subset \mathbb{R}^N$, and note that Π_C is piecewise continuously differentiable [26].

Accordingly, for the single integrator robot dynamics (4), our "move-to-projected-goal" law $\mathrm{u} : \mathcal{F} \to \mathbb{R}^N$ is defined as

$$\mathrm{u}(\mathrm{x}) = -k(\mathrm{x}-\overline{\mathrm{x}}^*), \tag{18}$$

where $k \in \mathbb{R}_{>0}$ is a fixed control gain, and we assume that $\mathcal{LF}(\mathrm{x})$ is continuously updated.

B. Qualitative Properties

We now continue with a list of its qualitative (continuity, existence & uniqueness, invariance and stability) properties.

Proposition 2 *The "move-to-projected-goal" law in (18) is piecewise continuously differentiable.*

Proof. An important property of power diagrams inherited from standard Voronoi diagrams [28] is that the boundary of a power cell is a piecewise continuously differentiable function of generator locations. Similarly, for any $\mathrm{x} \in \mathcal{F}$, we have that the boundary of the local free space $\mathcal{LF}(\mathrm{x})$ is piecewise continuously differentiable, because $\mathcal{LF}(\mathrm{x})$ is a nonempty erosion of the local workspace $\mathcal{LW}(\mathrm{x})$ by a fixed open ball, and $\mathcal{LW}(\mathrm{x})$ is an element of the power diagram of the workspace $\mathcal{W}$ generated by disks representing the robot and obstacles. Hence, one can conclude that the "move-to-projected-goal" law is piecewise continuously differentiable because metric projections onto (moving) convex cells are piecewise continuously differentiable [26], [29], [30], and the composition of piecewise continously differentiable functions are also piecewise continuously differentiable [31]. ■

Proposition 3 *The free space $\mathcal{F}$ in (1) is positively invariant under the "move-to-projected" law (18).*

Proof. By construction (16), for any $\mathrm{x} \in \mathcal{F}$, the "move-to-projected-goal" law always selects a safe local target location $\overline{\mathrm{x}}^*$ (17) such that the line segment between x and $\overline{\mathrm{x}}^*$ is free of collisions, because the local free space $\mathcal{LF}(\mathrm{x})$ is a collision free convex set (Lemma 1) and contains both x and $\overline{\mathrm{x}}^*$. Hence, at the boundary of $\mathcal{F}$, the robot either stays on the boundary or moves towards the interior of $\mathcal{F}$, but never crosses the boundary. ■

Proposition 4 *For any initial $\mathrm{x} \in \mathcal{F}$, the "move-to-projected-goal" law (18) has a unique continuously differentiable flow in $\mathcal{F}$ (1) defined for all future time.*

Proof. The existence, uniqueness and continuous differentiability of its flow follow from the Lipschitz continuity of the "move-to-projected-goal" law in its compact domain $\mathcal{F}$, because a piecewise continuously differentiable function is also locally Lipschitz on its domain [31], and a locally Lipschitz function on a compact set is globally Lipschitz on that set [32]. ■

Proposition 5 *The set of stationary points of the "move-to-projected-goal" law (18) is $\{\mathrm{x}^*\} \cup \{\mathrm{s}_i\}_{i\in\{1,2,\ldots,n\}}$, where*

$$\mathrm{s}_i := \mathrm{p}_i - (r+\rho_i)\frac{\mathrm{x}^*-\mathrm{p}_i}{\|\mathrm{x}^*-\mathrm{p}_i\|}. \tag{19}$$

Proof. It follows from (17) and (18) that the goal location x^* is a stationary point, because $\mathrm{x}^* \in \mathcal{LF}(\mathrm{x}^*)$. Note that, for any $\mathrm{x} \in \mathcal{F}$, if $\mathrm{x}^* \in \mathcal{LF}(\mathrm{x})$, then $\overline{\mathrm{x}}^* = \mathrm{x}^*$. Hence, in the sequel of the proof, we only consider the set of robot locations satisfying $\mathrm{x}^* \notin \mathcal{LF}(\mathrm{x})$.

To see that there is exactly one stationary point associated with each obstacle, for any $\mathrm{x} \in \mathcal{F}$, consider the power diagram $\mathcal{P}(\hat{\mathbf{p}}, \hat{\boldsymbol{\rho}}) = \{P_0, P_1, \ldots, P_n\}$ of $\mathcal{W}$ associated with $\hat{\mathbf{p}} = (\hat{\mathrm{p}}_0, \hat{\mathrm{p}}_1, \ldots, \hat{\mathrm{p}}_n) \in \mathcal{W}^{n+1}$ and $\hat{\boldsymbol{\rho}} = (\hat{\rho}_0, \hat{\rho}_1, \ldots, \hat{\rho}_n) \in (\mathbb{R}_{\geq 0})^{n+1}$ where $\hat{\mathrm{p}}_0 = \mathrm{x}$, $\hat{\rho}_0 = r$ and $\hat{\mathrm{p}}_i = \mathrm{p}_i$, $\hat{\rho}_i = \rho_i$ for all $i \neq 0$. Recall that $\mathcal{LW}(\mathrm{x}) = P_0$ and its boundary $\partial\mathcal{LW}(\mathrm{x})$ is defined by the boundary $\partial\mathcal{W}$ of $\mathcal{W}$ and the separating hyperplane H_{0i} between P_0 and P_i for some $i \neq 0$; and $\mathcal{LF}(\mathrm{x})$ is obtained by eroding $\mathcal{LW}(\mathrm{x})$ by an open disk of radius r. Further, because of the convexity of $\mathcal{W}$, observe from (17) that the projected goal $\overline{\mathrm{x}}^*$ satisfies that if $\mathrm{x}^* \notin \mathcal{LF}(\mathrm{x})$, then $d(\overline{\mathrm{x}}^*, H_{0i}) = r$ for some $i \neq 0$. Note

[13] In general, the metric projection of a point onto a convex set can be efficiently computed using a standard convex programming solver [24]. If $\mathcal{W}$ is a convex polytope, then the robot's local free space, $\mathcal{LF}(\mathrm{x})$, is also a convex polytope and can be written as a finite intersection of half-spaces. Hence, the metric projection onto a convex polytope can be recast as quadratic programming and can be solved in polynomial time [27]. In the case of a convex polygonal environment, $\mathcal{LF}(\mathrm{x})$ is a convex polygon, and the metric projection onto a convex polygon can be solved analytically, because the solution lies on one of its edges unless the input point is inside the polygon.

that $d(\overline{\mathrm{x}}^*, H_{0i}) = r$ if and only if $d(\mathrm{p}_i, H_{i0}) = \rho_i$ (see (8)) and so $\|\overline{\mathrm{x}}^* - \mathrm{p}_i\| = r + \rho_i$.

We have from (8) that if $\|\mathrm{x} - \mathrm{p}_i\| > (r + \rho_i)$ then $d(\mathrm{x}, H_{0i}) > r$. Hence, if $d(\mathrm{x}, H_{0i}) = r$ (i.e., $d(\mathrm{p}_i, H_{i0}) = \rho_i$ and $\|\mathrm{x} - \mathrm{p}_i\| = r + \rho_i$) for some $i \neq 0$, then, since $\|\mathrm{p}_i - \mathrm{p}_j\| > (\rho_i + \rho_j + 2r)$ (Assumption 1), $\|\mathrm{x} - \mathrm{p}_j\| > r + \rho_j$ and so $d(\mathrm{x}, H_{0j}) > r$ for all $j \neq i$. Therefore, there is only one obstacle index i such that $\mathrm{x} = \overline{\mathrm{x}}^*$ and $d(\overline{\mathrm{x}}^*, H_{0i}) = r$ (i.e., $\|\overline{\mathrm{x}}^* - \mathrm{p}_i\| = r + \rho_i$). Further, since $\overline{\mathrm{x}}^*$ the unique optimal solution of (16), H_{0i} should be tangent to the level curves of squared distance $\|\mathrm{x} - \mathrm{x}^*\|^2$ [24], which is the case if x, p_i and x^* are all collinear. As a result, by eliminating one of such antipodal points around the obstacle, one can verify that the only stationary point s_i of (18) associated with ith obstacle is given by (19), which completes the proof. ■

Lemma 2 *The "move-to-projected-goal" law (18) in a small neighborhood of the goal* x^* *is given by*

$$\mathrm{u}(\mathrm{x}) = -k(\mathrm{x} - \mathrm{x}^*), \quad \forall\, \mathrm{x} \in B(\mathrm{x}^*, \epsilon), \tag{20}$$

for some $\epsilon > 0$*; and around the stationary point* s_i *(19), associated with obstacle* i*, it is given by*

$$\mathrm{u}(\mathrm{x}) = -k\left(\mathrm{x} - \mathrm{x}^* + \frac{(\mathrm{x} - \mathrm{p}_i)^{\mathrm{T}}(\mathrm{x}^* - \hat{\mathrm{h}}_i)}{\|\mathrm{x} - \mathrm{p}_i\|^2}(\mathrm{x} - \mathrm{p}_i)\right), \tag{21}$$

for all $\mathrm{x} \in B(\mathrm{s}_i, \varepsilon)$ *and some* $\varepsilon > 0$*, where* $\hat{\mathrm{h}}_i := \alpha_i \mathrm{x} + (1 - \alpha_i)\mathrm{p}_i$ *and* $\hat{\alpha}_i = \frac{1}{2} - \frac{r^2 - \rho_i^2}{2\|\mathrm{x} - \mathrm{p}_i\|^2} + \frac{r}{\|\mathrm{x} - \mathrm{p}_i\|}$. [14]

Proof. The result for the goal location x^* follows from the continuity of power diagrams and $\mathrm{x}^* \in \mathcal{LF}(\mathrm{x}^*)$.

To see the result for the stationary point s_i, recall from the proof of Proposition 5 that s_i lies on the boundary of $\mathcal{LF}(\mathrm{s}_i)$ defined by the separating hyperplane between the robot's power cell (i.e., local workspace) and ith obstacle's power cell, and has a certain clearance between the boundary segment of $\mathcal{LF}(\mathrm{s}_i)$ defined by the separating hyperplane between the robot's power cell and any other obstacle's power cell. Hence, using the continuity of power partitions, for any $\mathrm{x} \in B(\mathrm{s}_i, \varepsilon)$ the projected-goal $\overline{\mathrm{x}}^*$ can be located by taking the projection of x^* onto (a shifted version of) the separating hyperplane between the robot's power cell and ith obstacle's as

$$\overline{\mathrm{x}}^* = \mathrm{x}^* - \frac{(\mathrm{x} - \mathrm{p}_i)^{\mathrm{T}}(\mathrm{x}^* - \hat{\mathrm{h}}_i)}{\|\mathrm{x} - \mathrm{p}_i\|^2}(\mathrm{x} - \mathrm{p}_i), \tag{22}$$

which completes the proof. ■

Proposition 6 *The goal* x^* *is the only locally stable equilibrium of the "move-to-projected-goal" law (18), and all the stationary points,* s_i *(19), associated with obstacles are nondegenerate saddles.*

Proof. The goal x^* is a locally stable point of the "move-to-projected-goal" law, because its Jacobian at x^* is the diagonal matrix with all diagonal entries equal to $-k$ (Lemma 2).

[14] $\hat{\alpha}_i$ is a slightly different version of α_{ij} (7) because $\mathcal{LF}(\mathrm{x})$ is the erosion of $\mathcal{LW}(\mathrm{x})$ by the robot body radius r.

To determine the type of the stationary point s_i, without loss of generality, let $\mathrm{p}_i = (p_{i1}, 0, \ldots, 0) \in \mathbb{R}^N$ and $\mathrm{x}^* = (x_1^*, 0, \ldots, 0) \in \mathbb{R}^N$ such that $p_{i1} < x_1^*$, and so $\mathrm{s}_i = (s_{i1}, 0, \ldots, 0) \in \mathbb{R}^N$ satisfying $s_{i1} < p_{i1}$. Note that since $\mathrm{x}^* \in \mathcal{F}$ and $\|\mathrm{s}_i - \mathrm{p}_i\| = r + \rho_i$, we have $x_1^* - p_{i1} \geq p_{i1} - s_{i1} = r + \rho_i$ and so $x_1^* - s_{i1} \geq 2(p_{i1} - s_{i1})$. Hence, using (21), one can verify that the Jacobian matrix of the "move-to-projected-goal" at s_i is given by

$$\mathbf{J} = \left.\frac{\mathrm{du}(\mathrm{x})}{\mathrm{dx}}\right|_{\mathrm{x}=\mathrm{s}_i} = \begin{bmatrix} -k\frac{\rho_i}{r+\rho_i} & ? & ? & \ldots & ? \\ 0 & \beta & 0 & \ldots & 0 \\ \vdots & \ddots & \ddots & \ddots & \vdots \\ 0 & \ldots & 0 & \beta & 0 \\ 0 & \ldots & \ldots & 0 & \beta \end{bmatrix} \tag{23}$$

where $\beta = k\frac{x_1^* - p_{i1}}{r + \rho_i} \geq k$. Since it is in a triangular form, the eigenvalues of $\mathbf{J}$ are its diagonal elements. Therefore, s_i is the nondegenerate saddle point of the "move-to-projected-goal" law associated with ith obstacle, and this completes the proof. ■

Proposition 7 *The goal location* x^* *is an asymptotically stable equilibrium of the "move-to-projected-goal" law, whose basin of attraction includes* $\mathcal{F}$*, except a set of measure zero.*

Proof. Consider the squared Euclidean distance to the goal as a smooth Lyapunov function candidate, i.e., $V(\mathrm{x}) := \|\mathrm{x} - \mathrm{x}^*\|^2$, and it follows from (16) and (18) that

$$\dot{V}(\mathrm{x}) = -k \underbrace{2(\mathrm{x} - \mathrm{x}^*)^{\mathrm{T}}(\mathrm{x} - \overline{\mathrm{x}}^*)}_{\geq \|\mathrm{x} - \overline{\mathrm{x}}^*\|^2 \text{ since } \mathrm{x} \in \mathcal{LF}(\mathrm{x}) \text{ and } \|\mathrm{x} - \mathrm{x}^*\|^2 \geq \|\overline{\mathrm{x}}^* - \mathrm{x}^*\|^2}, \tag{24}$$

$$\leq -k\|\mathrm{x} - \overline{\mathrm{x}}^*\|^2 \leq 0, \tag{25}$$

which is zero if and only if x is a stationary point. Hence, we have from LaSalle's Invariance Principle [32] that all robot configurations in $\mathcal{F}$ asymptotically reach the set of equilibria of (18). Therefore, the result follows from Proposition 2 and Proposition 6 since x^* is the only stable stationary point of the piecewise continuous "move-to-projected-goal" law (18) and all other stationary points are nondegenerate saddles whose stable manifolds have empty interiors [33]. ■

Finally, we find it useful to summarize important qualitative properties of "move-to-projected-goal" law as:[15]

Theorem 1 *The piecewise continuously differentiable "move-to-projected-goal" law in (18) leaves robot's free space* $\mathcal{F}$ *(1) positively invariant, and its unique continuously differentiable flow, starting at almost any configuration* $\mathrm{x} \in \mathcal{F}$*, asymptotically reaches the goal location* x^**, while strictly decreasing the squared Euclidean distance to the goal,* $\|\mathrm{x} - \mathrm{x}^*\|^2$*, along the way.*

[15] Since the "move-to-projected-goal" law is piecewise continously differentiable, it can be lifted to higher order dynamical models [34]–[36].

C. An Extension for Differential Drive Robots

Consider a disk-shaped differential drive robot described by state $(\mathrm{x}, \theta) \in \mathcal{F} \times (-\pi, \pi]$, centered at $\mathrm{x} \in \mathcal{F}$ with body radius $r \in \mathbb{R}_{\geq 0}$ and orientation $\theta \in (-\pi, \pi]$, moving in $\mathcal{W}$. The kinematic equations describing its motion are

$$\begin{aligned} \dot{\mathrm{x}} &= v \begin{bmatrix} \cos\theta \\ \sin\theta \end{bmatrix}, \\ \dot{\theta} &= \omega, \end{aligned} \tag{26}$$

where $v \in \mathbb{R}$ and $\omega \in \mathbb{R}$ are, respectively, the linear (tangential) and angular velocity inputs of the robot.

In contrary to the "move-to-projected-goal" law of a fully actuated robot in (18), a differential drive robot can not directly move towards the projected goal $\overline{\mathrm{x}}^*$ (17) of a given goal location $\mathrm{x}^* \in \mathring{\mathcal{F}}$, unless it is perfectly aligned with $\overline{\mathrm{x}}^*$, because it is underactuated due to the nonholonomic constraint $\begin{bmatrix} -\sin\theta \\ \cos\theta \end{bmatrix}^{\mathrm{T}} \dot{\mathrm{x}} = 0$. [16] In consequence, to determine a linear velocity input that guarantees collision avoidance and conforms to the nonholonomic constraint, we select a safe target location that satisfies the following convex optimization problem,

$$\begin{aligned} &\text{minimize} && \|\mathrm{q} - \mathrm{x}^*\|^2 \\ &\text{subject to} && \mathrm{q} \in \mathcal{LF}(\mathrm{x}) \cap H_N \end{aligned} \tag{27}$$

where

$$H_N := \left\{ \mathrm{q} \in \mathcal{W} \middle| \begin{bmatrix} -\sin\theta \\ \cos\theta \end{bmatrix}^{\mathrm{T}} (\mathrm{q} - \mathrm{x}) = 0 \right\} \tag{28}$$

is the straight line motion range due to the nonholonomic constraint. Note that $\mathcal{LF}(\mathrm{x}) \cap H_N$ is a closed line segment in $\mathcal{W}$. Hence, once again, the unique solution of (27) is given by

$$\overline{\mathrm{x}}^*_v := \begin{cases} \mathrm{x}^* & \text{, if } \mathrm{x}^* \in \mathcal{LF}(\mathrm{x}) \cap H_N, \\ \Pi_{\mathcal{LF}(\mathrm{x}) \cap H_N}(\mathrm{x}^*) & \text{, otherwise,} \end{cases} \tag{29}$$

where Π_C is the metric projection map onto a convex set C. Similarly, to determine the robot's angular motion, we select another safe target location that solves

$$\begin{aligned} &\text{minimize} && \|\mathrm{q} - \mathrm{x}^*\|^2 \\ &\text{subject to} && \mathrm{q} \in \mathcal{LF}(\mathrm{x}) \cap H_G \end{aligned} \tag{30}$$

where

$$H_G := \left\{ \omega \mathrm{x} + (1-\omega)\,\mathrm{x}^* \in \mathcal{W} \middle| \ \omega \in \mathbb{R} \right\} \tag{31}$$

is the line segment of $\mathcal{W}$ containing x and x^*, and the unique solution of (30) is

$$\overline{\mathrm{x}}^*_\omega := \begin{cases} \mathrm{x}^* & \text{, if } \mathrm{x}^* \in \mathcal{LF}(\mathrm{x}) \cap H_G, \\ \Pi_{\mathcal{LF}(\mathrm{x}) \cap H_G}(\mathrm{x}^*) & \text{, otherwise.} \end{cases} \tag{32}$$

Accordingly, based on a standard differential drive controller [37], we propose the following "move-to-projected-goal" law for a differential drive robot,[17] [18]

$$v = -k \begin{bmatrix} \cos\theta \\ \sin\theta \end{bmatrix}^{\mathrm{T}} (\mathrm{x} - \overline{\mathrm{x}}^*_v), \tag{33a}$$

$$\omega = k \ \mathrm{atan}\left(\frac{\begin{bmatrix} -\sin\theta \\ \cos\theta \end{bmatrix}^{\mathrm{T}} \left(\mathrm{x} - \frac{\overline{\mathrm{x}}^*_\omega + \overline{\mathrm{x}}^*}{2} \right)}{\begin{bmatrix} \cos\theta \\ \sin\theta \end{bmatrix}^{\mathrm{T}} \left(\mathrm{x} - \frac{\overline{\mathrm{x}}^*_\omega + \overline{\mathrm{x}}^*}{2} \right)} \right), \tag{33b}$$

where $k > 0$ is fixed and $\overline{\mathrm{x}}^*$ is the projected goal as defined in (17).

We summarize some important properties of the "move-to-projected-goal" law of a differential drive robot as:

Proposition 8 *The "move-to-projected-goal" law of a disk-shaped differential drive robot in (33) asymptotically steers almost all configurations in its positively invariant domain $\mathcal{F} \times (-\pi, \pi]$ towards any given goal location $\mathrm{x}^* \in \mathring{\mathcal{F}}$, without increasing the Euclidean distance to the goal along the way.*

Proof. The positive invariance of $\mathcal{F} \times (-\pi, \pi]$ under the "move-to-projected-goal" law (33) and the existence and uniqueness of its flow can be established using similar patterns of the proofs of Proposition 2, Proposition 3 and Proposition 4, and the flow properties of the differential drive controller in [37].

Using the squared distance to goal, $V(\mathrm{x}) = \|\mathrm{x} - \mathrm{x}^*\|^2$, as a smooth Lypunov function candidate, one can establish the stability properties from (26), (27) and (33) as follows: for any $(\mathrm{x}, \theta) \in \mathcal{F} \times (-\pi, \pi]$

$$\dot{V}(\mathrm{x}) = -k \underbrace{2(\mathrm{x} - \mathrm{x}^*)^{\mathrm{T}} (\mathrm{x} - \overline{\mathrm{x}}^*_v)}_{\substack{\geq \|\mathrm{x} - \overline{\mathrm{x}}^*_v\|^2 \\ \text{since } \mathrm{x} \in \mathcal{LF}(\mathrm{x}) \cap H_N \text{ and } \|\mathrm{x} - \mathrm{x}^*\|^2 \geq \|\overline{\mathrm{x}}^*_v - \mathrm{x}^*\|^2}}, \tag{34}$$

$$\leq -k \|\mathrm{x} - \overline{\mathrm{x}}^*_v\|^2 \leq 0. \tag{35}$$

Hence, it follows from LaSalle's Invariance Principle [32] that all configurations in $\mathcal{F} \times (-\pi, \pi]$ asymptotically reach the set of configurations where robots are located at the associated projected goal $\overline{\mathrm{x}}^*_v$ at any arbitrary orientation,

$$\left\{ (\mathrm{x}, \theta) \in \mathcal{F} \times (-\pi, \pi] \middle| \mathrm{x} = \overline{\mathrm{x}}^*_v \right\}. \tag{36}$$

Note that, for any fixed $\overline{\mathrm{x}}^*_v$, $\overline{\mathrm{x}}^*_\omega$ and $\overline{\mathrm{x}}^*$, the standard differential drive controller asymptotically aligns the robot with $\frac{\overline{\mathrm{x}}^*_\omega + \overline{\mathrm{x}}^*}{2}$, i.e., $\begin{bmatrix} -\sin\theta \\ \cos\theta \end{bmatrix}^{\mathrm{T}} \left(\mathrm{x} - \frac{\overline{\mathrm{x}}^*_\omega + \overline{\mathrm{x}}^*}{2} \right) = 0$. Hence, using (16), (27) and (30), one can conclude that $\overline{\mathrm{x}}^*_v = \overline{\mathrm{x}}^*_\omega = \overline{\mathrm{x}}^*$, whenever $\mathrm{x} = \overline{\mathrm{x}}^*_v$ and $\begin{bmatrix} -\sin\theta \\ \cos\theta \end{bmatrix}^{\mathrm{T}} \left(\mathrm{x} - \frac{\overline{\mathrm{x}}^*_\omega + \overline{\mathrm{x}}^*}{2} \right) = 0$.

Therefore, using a similar approach to the proofs of Proposition 5, Lemma 2 and Proposition 6, one can verify that the set of stationary points of (33) is given by

$$\{\mathrm{x}^*\} \times (-\pi, \pi] \bigcup \left\{ (\mathrm{s}_i, \theta) \in \mathcal{F} \times (-\pi, \pi] \middle| \begin{bmatrix} -\sin\theta \\ \cos\theta \end{bmatrix}^{\mathrm{T}} (\mathrm{s}_i - \mathrm{x}^*) = 0 \right\}, \tag{37}$$

[16] Here, $\mathring{\mathcal{F}}$ denotes the interior of $\mathcal{F}$, and we particularly require the goal location to be in $\mathring{\mathcal{F}}$ to guarantee that a robot can nearly align its orientation with the (local) goal location in finite time.

[17] We follow [37] by resolving the indeterminacy through setting $\omega = 0$ whenever $\mathrm{x} = \frac{\overline{\mathrm{x}}^*_\omega + \overline{\mathrm{x}}^*}{2}$. Note that this introduces the discontinuity necessitated by Brockett's condition [38].

[18] In the design of angular motion, we particularly select a local target location, $\frac{\overline{\mathrm{x}}^*_\omega + \overline{\mathrm{x}}^*}{2} \in \mathring{\mathcal{F}}$ given $\mathrm{x}^* \in \mathring{\mathcal{F}}$, in the interior $\mathring{\mathcal{F}}$ of $\mathcal{F}$ to increase the convergence rate of the resulting vector field. One can consider other convex combinations of $\overline{\mathrm{x}}^*_\omega$ and $\overline{\mathrm{x}}^*$, and the resulting vector field retains qualitative properties.

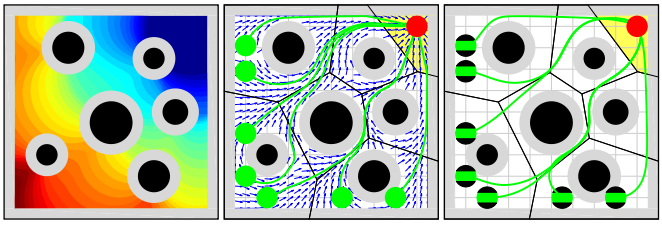

Fig. 3. (left) The Euclidean distance, $\|\overline{\mathrm{x}}^* - \mathrm{x}^*\|$, between the projected goal, $\overline{x}^*$, and the goal, x^*, as a function of robot location. Example trajectories of the "move-to-projected-goal" law starting at a set of initial configurations (green) towards the goal location (red) for (middle) a fully actuated and (right) a differential drive robot.

where s_i is defined as in (19); and every robot configuration located at x^* is locally stable and all stationary points associated with obstacles are nondegenerate saddles with stable manifolds of measure zero. Thus, the result follows. ■

V. Numerical Simulations

To demonstrate the motion pattern of our "move-to-projected-goal" law around a goal location, we consider a 10×10 environment populated with disk-shaped obstacles, and a goal located at around its upper right corner, as illustrated in Fig. 3. [19] On the middle and right of Fig. 3, respectively, we present example trajectories of the "move-to-projected-goal" law for a fully actuated and a differential drive robot. It is really fascinating to observe such a significant consistency between the resulting trajectories and the boundary of the power diagram of the environment, generated by the robot at the goal and obstacles. Note that the boundary of a power diagram is the safest region away from obstacles according to the power distance. Although they are initiated at the same location, as seen in Fig. 3, a fully actuated and a differential drive robot may follow significantly different trajectories due to their differences in system dynamics and controller design. We also would like to note that the "move-to-projected-goal" law decreases not only the Euclidean distance, $\|\mathrm{x} - \mathrm{x}^*\|$, to the goal, but also the Euclidean distance, $\|\overline{\mathrm{x}}^* - \mathrm{x}^*\|$, between the projected goal, $\overline{\mathrm{x}}^*$, and the global goal, x^*, as illustrated on the left of Fig. 3.

To demonstrate the behaviour of the "move-to-projected-goal" law far away from a goal location, we consider a 50×10 environment cluttered with obstacles, and a goal located at around its upper left corner, as illustrated in Fig. 4. We present in Fig. 4 example trajectories of the "move-to-projected-goal" law for a fully actuated and a differential drive robot. Once again, the resulting flow is significantly consistent with the boundary of the power diagram of the environment. This might have a value for certain practical settings where a robot requires to balance its distance to nearby obstacles while navigating towards its destination.

[19] For all simulations we set $k = 1$, and all simulations are obtained through numerical integration of the associated "move-to-projected-goal" law using the `ode45` function of MATLAB.

VI. Conclusion

In this paper, we introduce a novel use of power diagrams for identifying a convex collision free neighborhood of a robot configuration, and propose a convex optimization framework whose continuous evaluation is used to solve the collision free robot navigation problem in a locally sensed metric sphere world, comprising the central contributions of the paper. The resulting vector field has a smooth flow with a unique attractor at a designated goal location, along with one saddle associated with each obstacle. Since all of its critical points are nondegenerate, our vector field asymptotically steers almost all configurations in the robot's free space to the goal location, with the guarantee of no collisions along the way. We also present its extensions for the widely used differential drive model, and demonstrate the effectiveness of the proposed navigation algorithm in numerical simulations.

Work now in progress targets navigation among convex obstacles with continuously differentiable boundaries, and robot navigation using a fixed radius sensory footprint. We are also exploring alternative partitioning methods with similar nice properties to power diagrams, and another possible extension for multirobot feedback motion design.

Acknowledgment

This work was supported by AFOSR under the CHASE MURI FA9550-10-1-0567.

References

[1] H. Choset, K. M. Lynch, S. Hutchinson, G. A. Kantor, W. Burgard, L. E. Kavraki, and S. Thrun, *Principles of Robot Motion: Theory, Algorithms, and Implementations*. Cambridge, MA: MIT Press, 2005.

[2] S. M. LaValle, *Planning Algorithms*. Cambridge, U.K.: Cambridge University Press, 2006.

[3] H. Choset and J. Burdick, "Sensor-based exploration: The hierarchical generalized Voronoi graph," *The International Journal of Robotics Research*, vol. 19, no. 2, pp. 96–125, 2000.

[4] D. Conner, H. Choset, and A. Rizzi, "Flow-through policies for hybrid controller synthesis applied to fully actuated systems," *Robotics, IEEE Transactions on*, vol. 25, no. 1, pp. 136–146, 2009.

[5] O. Khatib, "Real-time obstacle avoidance for manipulators and mobile robots," *The International Journal of Robotics Research*, vol. 5, no. 1, pp. 90–98, 1986.

[6] D. Koditschek, "Exact robot navigation by means of potential functions: Some topological considerations," in *Robotics and Automation, 1987 IEEE International Conference on*, vol. 4, 1987, pp. 1–6.

[7] E. Rimon and D. Koditschek, "Exact robot navigation using artificial potential functions," *Robotics and Automation, IEEE Transactions on*, vol. 8, no. 5, pp. 501–518, 1992.

[8] C. I. Connolly and R. A. Grupen, "The applications of harmonic functions to robotics," *Journal of Robotic Systems*, vol. 10, no. 7, pp. 931–946, 1993.

[9] G. Lionis, X. Papageorgiou, and K. Kyriakopoulos, "Locally computable navigation functions for sphere worlds," in *Robotics and Automation, 2007 IEEE International Conference on*, 2007, pp. 1998–2003.

[10] I. Filippidis and K. Kyriakopoulos, "Adjustable navigation functions for unknown sphere worlds," in *Decision and Control and European Control Conference, 2011 50th IEEE Conference on*, 2011, pp. 4276–4281.

[11] H. Tanner and K. Kyriakopoulos, "Nonholonomic motion planning for mobile manipulators," in *Robotics and Automation, 2000 IEEE International Conference on*, 2000, pp. 1233–1238.

[12] G. Roussos, D. Dimarogonas, and K. Kyriakopoulos, "3d navigation and collision avoidance for a non-holonomic vehicle," in *American Control Conference, 2008*, 2008, pp. 3512–3517.

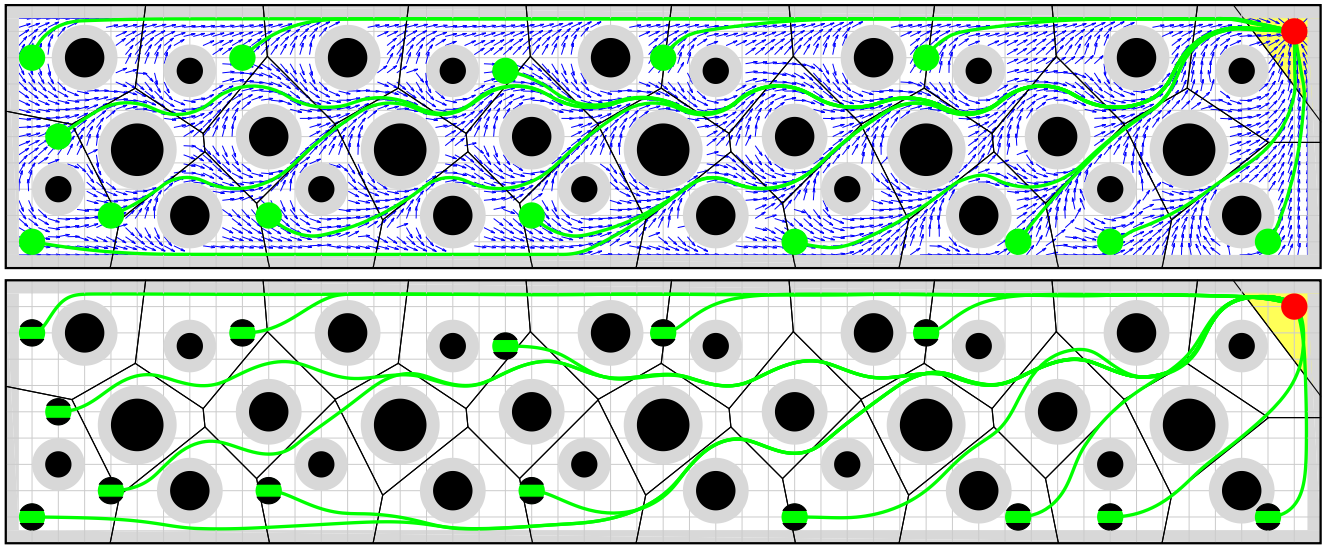

Fig. 4. Example trajectories of the "move-to-projected-goal" law for a fully actuated (top) and a differential drive (bottom) robot starting at a set of initial configurations (green) towards a desired goal location (red).

[13] R. R. Burridge, A. A. Rizzi, and D. E. Koditschek, "Sequential composition of dynamically dexterous robot behaviors," *The International Journal of Robotics Research*, vol. 18, no. 6, pp. 535–555, 1999.

[14] D. Conner, H. Choset, and A. Rizzi, "Integrating planning and control for single-bodied wheeled mobile robots," *Autonomous Robots*, vol. 30, no. 3, pp. 243–264, 2011.

[15] D. E. Koditschek and E. Rimon, "Robot navigation functions on manifolds with boundary," *Advances in Applied Mathematics*, vol. 11, no. 4, pp. 412 – 442, 1990.

[16] F. Aurenhammer, "Power diagrams: Properties, algorithms and applications," *SIAM Journal on Computing*, vol. 16, no. 1, pp. 78–96, 1987.

[17] C. Ó'Dúnlaing and C. K. Yap, "A retraction method for planning the motion of a disc," *Journal of Algorithms*, vol. 6, no. 1, pp. 104 – 111, 1985.

[18] J. Cortés, S. Martınez, T. Karatas, and F. Bullo, "Coverage control for mobile sensing networks," *Robotics and Automation, IEEE Transactions on*, vol. 20, no. 2, pp. 243–255, 2004.

[19] A. Kwok and S. Martnez, "Deployment algorithms for a power-constrained mobile sensor network," *International Journal of Robust and Nonlinear Control*, vol. 20, no. 7, pp. 745–763, 2010.

[20] L. Pimenta, V. Kumar, R. Mesquita, and G. Pereira, "Sensing and coverage for a network of heterogeneous robots," in *Decision and Control, 2008 47th IEEE Conference on*, 2008, pp. 3947–3952.

[21] O. Arslan and D. E. Koditschek, "Voronoi-based coverage control of heterogeneous disk-shaped robots," in *Robotics and Automation, 2016 IEEE International Conference on (accepted)*, 2016, http://arxiv.org/abs/1509.03842.

[22] E. Rimon and D. E. Koditschek, "The construction of analytic diffeomorphisms for exact robot navigation on star worlds," *Transactions of the American Mathematical Society*, vol. 327, no. 1, pp. 71–116, 1991.

[23] R. Haralick, S. R. Sternberg, and X. Zhuang, "Image analysis using mathematical morphology," *Pattern Analysis and Machine Intelligence, IEEE Transactions on*, vol. PAMI-9, no. 4, pp. 532–550, 1987.

[24] S. Boyd and L. Vandenberghe, *Convex Optimization*. Cambridge University Press, 2004.

[25] J. Munkres, *Topology*, 2nd ed. Pearson, 2000.

[26] L. Kuntz and S. Scholtes, "Structural analysis of nonsmooth mappings, inverse functions, and metric projections," *Journal of Mathematical Analysis and Applications*, vol. 188, no. 2, pp. 346 – 386, 1994.

[27] M. Kozlov, S. Tarasov, and L. Khachiyan, "The polynomial solvability of convex quadratic programming," *USSR Computational Mathematics and Mathematical Physics*, vol. 20, no. 5, pp. 223–228, 1980.

[28] F. Bullo, J. Cortés, and S. Martinez, *Distributed Control of Robotic Networks: A Mathematical Approach to Motion Coordination Algorithms*. Princeton University Press, 2009.

[29] A. Shapiro, "Sensitivity analysis of nonlinear programs and differentiability properties of metric projections," *SIAM Journal on Control and Optimization*, vol. 26, no. 3, pp. 628–645, 1988.

[30] J. Liu, "Sensitivity analysis in nonlinear programs and variational inequalities via continuous selections," *SIAM Journal on Control and Optimization*, vol. 33, no. 4, pp. 1040–1060, 1995.

[31] R. W. Chaney, "Piecewise C^k functions in nonsmooth analysis," *Nonlinear Analysis: Theory, Methods & Applications*, vol. 15, no. 7, pp. 649 – 660, 1990.

[32] H. K. Khalil, *Nonlinear Systems*, 3rd ed. Prentice Hall, 2001.

[33] M. W. Hirsch, S. Smale, and R. L. Devaney, *Differential Equations, Dynamical Systems, and an Introduction to Chaos*, 2nd ed. Academic press, 2003.

[34] D. E. Koditschek, "Adaptive techniques for mechanical systems," in *Proc. 5th. Yale Workshop on Adaptive Systems*, 1987, pp. 259–265.

[35] ——, "Some applications of natural motion control," *Journal of Dynamic Systems, Measurement, and Control*, vol. 113, pp. 552–557, 1991.

[36] R. Fierro and F. L. Lewis, "Control of a nonholomic mobile robot: Backstepping kinematics into dynamics," *Journal of Robotic Systems*, vol. 14, no. 3, pp. 149–163, 1997.

[37] A. Astolfi, "Exponential stabilization of a wheeled mobile robot via discontinuous control," *Journal of dynamic systems, measurement, and control*, vol. 121, no. 1, pp. 121–126, 1999.

[38] R. W. Brockett, *Asymptotic stability and feedback stabilization*. Defense Technical Information Center, 1983.